STUDY OF MICRODEFORMATIONS OF CONCRETE BY COHERENT OPTICAL TECHNIQUES

P.M.BOONE (*), M.H.DE CALUWE (**),
D.A. VAN NIEUWENBURG (***)

COMMISSION V - W.G.4

1. INTRODUCTION

The knowledge of the deformation behaviour of concrete is of major importance in the design of concrete constructions. This behaviour has so far only been verified under macroscopic, practical situations. One of the reasons therefore is that the available mathematical models have been derived from a large number of experimental findings, the macroscopic deformations due to the external loads considered in the calculations are in fact the summation of microscopic deformations of the different constituents of the heterogeneous material called concrete. Up to now little information is available on the deformational behaviour of the different constituents.

The use of coherent optical techniques allows one to investigate microscopic deformations, and can give information about the interaction of the individual components.
The phenomena investigated were:

1. the deformation properties of the mortar matrix and the aggregate during the shrinkage period.
2. micro cracking under static load.
3. the atmospheric sensitivity of different concrete compositions after drying.

The coherent optical techniques available are holography and speckle correlation; incoherent techniques are high frequency moiré, white light speckling and photoelasticity.

This article will only deal with holography; and its usefulness in the study of concrete, with the restriction that only hypotheses were derived from this general survey and must serve as a base for more extensive research.

(*) Associate Professor, Lab. Soete for Strength of Materials, University Ghent, BELGIUM
(**) Chief Technician, Seminar for Mechanics of Machines, University Ghent, BELGIUM
(***) Chief Assistant, Lab. Magnel for Reinforced Concrete, University Ghent, BELGIUM

2. GENERAL REMARKS

The principles of holographic interferometry are supposed to be known, so that we can concentrate on the set-ups for the specific tests. Real time holographic interferometry is very useful in nondestructive testing, as it allows easy detection of small deformations by observing the fringes passing by over the investigated area, and the adaptation of the fringe pattern to the magnitude of a possible defect. It also allows the repetition of loading cycles with eventual readjustment of the optical set-up.

Experiments were carried out in order to the study of the behaviour of concrete to uniaxial compression and bending, and to investigate shrinkage deformations and the influence of varying atmospheric conditions. The specific set-ups used are described later.
The laser used was a Spectra Physics 165 Argon Ion Laser producing 1 W TEMoo single line, single frequency operation at 514,5 nm by the use of an intracavity etalon.

For all tests, except those on the atmospheric susceptibility, the specimens were made from a reference concrete with composition:

- gravel 7/14	1.060 kg
- gravel 4/7	190 kg
- sand 2/5	100 kg
- sand 0/2	535 kg
- cement P40	350 kg
- water	160 l

Volumic mass of the compacted fresh concrete: 2400 kg/m^3.

The specimen were cast in steel moulds and were compacted on a vibration table. Demoulding was carried out 24 hours after casting, followed by storing for another 14 hours in a controlled climate (temp. 20°C ± 1°C, humidity : 90%,± 2%)

3. EXPERIMENTS

a. Shrinkage test:

The test was performed on 4 cubes (side length 100 mm). First, the surface which was investigated during the test, was ground.
During the test, the deformation of two reference prisms (100 x 100 x 400 mm) were measured dayly on 4 sides with a mechanical deformeter (Whitemore,

gauge length 200 mm); one in a conditioned room (20°C ± 1°C, 60% ±3% R.H.) and the other in the holographic lab (20 to 22°C, 35 to 60% R.H.). Results of the shrinkage measurements are shown on fig. 1 (the lower curve referring to the "hololab" conditions).

The optical set-up was arranged so that the observation direction coincided with the illumination direction, and thus with the sensitivity vector. To achieve this, the object beam was directed onto the specimen surfaces via adjustable beamsplitter BS1, M1, diverging lens L2 and half silvered mirror BS2 (fig. 2). The reference beam path was directed towards the hologram plate H (8 E56 HD Holotest - Agfa Gevaert) via mirror M2 and diverging lens L1 .

In real time holographic interferometry, a reference hologram is taken at a determined loading state and is replaced in its fixture after processing, preferably at exactly the same location (accuracy: 0,1 µm). Although on first sight it looks quite difficult, this is easily achieved with a very simple plate holder. By changing the ratio of the beams'intensities, maximal contrast between the fringes formed by the actual image and the holographic one can be obtained.
Observation was possible through the viewfinder of still picture camera C (Hasselblad 500C with S-Planar 135 mm and extension bellows), allowing recording of interesting images whenever needed. Together with the interferogram, atmospheric conditions, date and time were recorded on the photographic negative by photographing the appropriate instruments on the same negative.
Each test cube was laid on 3 steel balls, fitted on a sturdy base plate so that the dimensional changes of the cube were not hampered. Atmospheric conditions of the lab were recorded daily, when the real time interferogram was recorded.

The first reference hologram was taken 48 hours after casting. Fig. 3 shows the situation 24 hours later. The fringe aspect is rather chaotic due to difference in shrinkage between the granulate and the mortar. However, deformation concentrations are visible in specific areas. The fringe number increases with increasing time up to a moment where they become hardly distinguishable (after 9 days). By taking a new "reference", we can continue the observations. Fig. 4 shows the final fringe pattern (after 32 days) referred to the situation 23 days earlier.

To illustrate the interpretation of the fringe pattern, fig. 5 shows a plot of the fringe number compared to the distance along the diagonal of the extreme left cube of fig. 4.
The interpretation of the complex fringe pattern is difficult but the use of a fringe concentration factor $Fc = \frac{a}{A}$, where a and A are respectively the smallest and largest fringe interdistance, is a simple and handy method to describe the deformations.

During the first week we observed a rapid dimensional change of the mortar. Although holography, as applied here, does not show the direction of that movement, one may expect shrinkage. The aggregates however remained roughly in place. Shear stresses will thus build up on the granulate - mortar boundaries. These are limited to a specific location and tend to concentrate along lines at the surface. Only after some time - probably when the shear stresses exceed a certain value - the aggregates begin to displace (probably outward).

Fc reaches a value of 0,1 after ten days and remains mainly constant thereafter. This means that the maximal out of plane difference would be roughly $10 \frac{\lambda}{2} = 2{,}71$ µm.

It was confirmed (by penetrants and binocular investigation) that at that level of shrinkage, microcracks have been formed at the boundaries of aggregate and mortar.

b. Monoaxial Compression Tests:

Rigid body movements of test specimen often mask the deformation fringes one is looking for. A beam steering instrument was incorporated in the set-up for compensation. The same set-up used for compression tests was used for atmospheric tests and bending.

The object beam impinges on the test surface under a small angle so that the sensitivity vector is not perpendicular to it. This is of minor importance as one only wants to look for cracks, which means abrupt discontinuities in the fringe pattern (qualitative measurements).

The set-up is represented schematically in fig. 6. The beam is split with variable beamsplitter BS into an object and a reference beam so that a 1:1 intensity ratio can be realized on the hologram plate H.

The objectbeam passes over M2 to a pinhole-lens unit to form a clean, diverging beam. The beam steering instrument is formed by convex lens L2 which is movable along the optical axis and plane mirror M3 rotatable along the vertical and horizontal axis.

Moving L2 alters the curvature of the wavefront and inclining M3 tilts it in any direction. That is definitely what the rigid body movements do and so one can always adapt the original wavefront to the tilt of the specimen. In practice, microscrews are adjusted until one finds the best zero fringe (bull eye) with an unchanged loading condition.

The reference beam passes over L3 and M4 to the holographic plate.
The reference hologram can be taken at zero load or at a determined static load. After processing, the plate is replaced in its fixture.

Generally, the fringes are not exactly cancelled as the emulsion of the holographic plate shrinks. Changing the position of L2 can compensate this. The fringe pattern is observed via the video camera VC, is recorded on tape by videorecorder VR and displayed on the monitor VD. Adjustment of the luminiscence and contrast potentiometers can enhance fringe visibility, as does the tuning of the diaphragm in photographic recording.
The pictures shown from here on are taken from the videoscreen. The quality is indeed worse than in direct photography but the flexibility of the video arrangement, the ease of work, the reproducibility of the test course and the documentary value of the tape greatly surpasses this drawback.

Specimens for compression tests were made from the same material as those for the shrinkage tests. Cubes of 200 mm side length were cast and tested after 32 days of drying under controlled climate conditions. Material defects due to shrinkage during that period were comparable to those detected during the previous experiments, which means microcracks already were present.

A small hydraulic compression machine specially made for this purpose was used. The load was alphanummerically recorded on the videotape, together with the fringe image.

At a load of only 4 kN, one can easily see discontinuities in the fringe pattern (fig. 7). Fig. 7a and 7b are different representations of the fringe pattern at the same load, illustrating the usefulness of the beam steering instrument.

Indeed, the fringe pattern of fig. 7b at zero tilt and rotation can hardly be evaluated, whereas fig. 7a (with some object beam tilt introduced), shows clearly fringe discontinuities in the vicinity of microcracks.
The large number of horizontal fringes are not due to deformation but to a correction in the object beam direction.

It is clear that microcracks are visible even at this low load level.

Further increase in load shows crack growth and rotation of aggregates together with out of plane movements. Near ultimate load (440 kN) some aggregates show fringe intervals of 2 mm while in the mortar they become undistinguishable. The fringe concentration factor becomes ≧ 0,01.

c. Bending:

The advantage of holography in nondestructive testing lies also in the possibility of the application of small loads, due to its great sensitivity. One can take full profit of this feature in the bending test.
A beam of 100 x 100 x 1000 mm also cast from the same standard mixture, was placed on two rollers (Ø 50 mm) fastened 800 mm apart in the test area of the foregoing set-up.
The beam had never been loaded before and was dried under the same conditions as the compression specimens. Loading was achieved by weights at the midpoint between the two rollers.
Fig. 8 represents the fringe pattern on the central part of the beam resulting from a load of no more than 450 N. The arrow indicates a fringe discontinuity which was first noticable at only 200 N load. A bending test till rupture confirmed that the rupture started from that crack.

d. Atmospheric sensitivity:

These tests were carried out on samples machined from existing road surfaces where problems were noticed after two years'service (h=250 mm, Ø 100 mm - diamond crown drilling).
The aggregate was natural lime stone, no other data were available. It was the opportunity to compare the atmospheric sensitivity of two different samples with respect to the reference concrete.

Both specimens were stuck with epoxy glue on a heavy steel baseplate and put into the test area. A reference hologram was taken.

After 24 hours under atmospheric laboratory conditions, the fringe pattern of fig. 9 became visible, both pictures being corrected for rigid body movements. Note that no load at all has been applied to the specimen.
Both specimens showed a remarkably rapid formation of fringes, whereas the reference cubes showed almost no fringes over the same period of time, which means that the lime stone is more susceptible to atmospheric changes than the gravel and shingle used in the reference concrete. One specimen showed fringe concentrations between the upper layer and the body which later gave evidence of a large crack (see arrow on fig. 9).
Furthermore, both specimens had no noticable difference in atmospheric sensitivity.

4. GENERAL CONCLUSIONS

It became evident that microcracks and local deformations are formed in concrete during the drying process.
These effects occur on the microscopic scale with respect to the dimensions of the composing materials. This does by no means mean that they determine the strength of the material on the macroscopic scale. It only explains where and how cracks, and even rupture, could start.

A comparable statement holds for metals as well (seen on the corresponding microscopic scale), as illustrated in fig. 11 where we have carried out an experiment with High Frequency-Moiré on an aluminium tensile specimen with large cristals. It is clear that the cristals deform heterogeneously as well, although this remains unnoticed in regular tensile tests.

We can conclude that holographic interferometry is generally too sensitive for measurements on concrete under practical loads, although interesting findings have been made on the deformational behaviour of the material at low stress levels. Microcrack detection however is possible with this sensitivity and is easy to carry out. Comparison between different kinds of samples can tell much about their atmospherical sensitivity and requires no manipulation of the samples at all.
It has been shown by the experiments on the road concrete that the latter deformations are of the same order of magnitude than those due to elastic loading; this could be a partial explanation of the corrosion phenomenon.

Finally, the beam steering instrument has proven to be an excellent tool in nondestructive testing, allowing elimination of rigid body movement fringes.

5. ACKNOWLEDGEMENTS

The authors thank the Belgian Fund for Collective Fundamental Research for grant nr. 2.0014.81, that allowed this work to be undertaken.

6. REFERENCES

1) PFLUG, L.: "Application of Optical Methods to Crack Detection in Bended Concrete Beams" Proc. of 7th Nat. Congress of the Italian Faculty for Stress Analysis (A.I.A.S.) Cagliari, 26-29 sept. 1979

2) LIGHT, M.F.; LUXMORE, A.R.: "Detection of Cracks in Concrete by Holography", Mq. Conc.Res., 24, 167-172 (1972)

3) LIGHT, M.F.; LUXMOORE, A.R.:"Crack Detection by Holography" Journal Precast Concrete, 4, 26-28 (1973)

4) STROEVEN P.; DE HAAS, H.M.: "Crack Detection Techniques in Concrete Materials Research", 10th Annual Conference of the British Society for Strain Measurement 16-19 sept. 1974 (Univ. of Warwick)

5) DALHUISEN, P.H.; STROEVEN P.: "Analyse der Rissbildung in Kalksandstein- mauerwerk mittels der Holographischen Interferometrie" Proc. Symp. Brugge 26-28 Apr. 1976

6) SPEIZLER, H.; SCHOLZ, C.H.; LU, C.P.J.: "Strain and Creep Measurements on Rocks by Holographic Interferometry", Pure Appl. Geophys., 112/3, 571-582 (1974)

7) VAN NIEUWENBURG, D.; DE CALUWE, M.; BOONE, P.: "Fundamentele studie van het Vervormingsgedrag van Beton via Koherent-Optische Technieken", FKFO nr. 2.0014.81, Progress Report (1982)

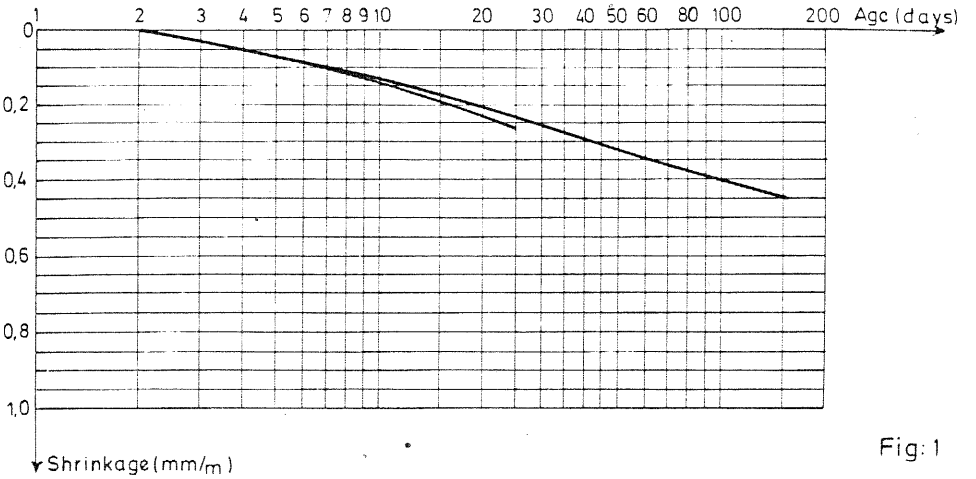

Fig: 1

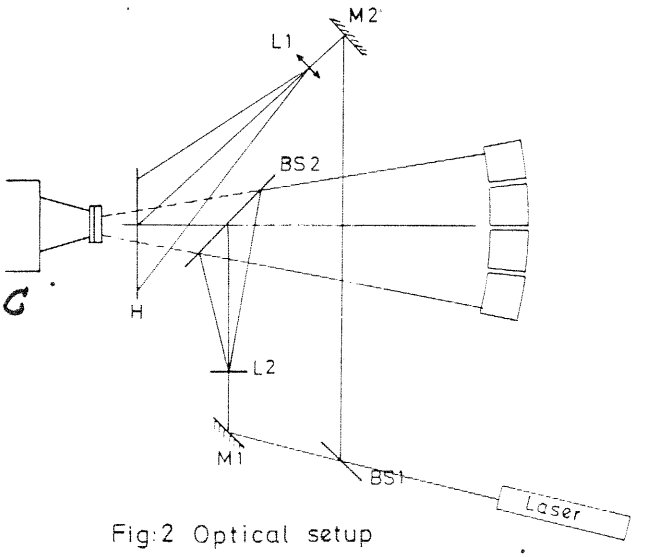

Fig: 2 Optical setup

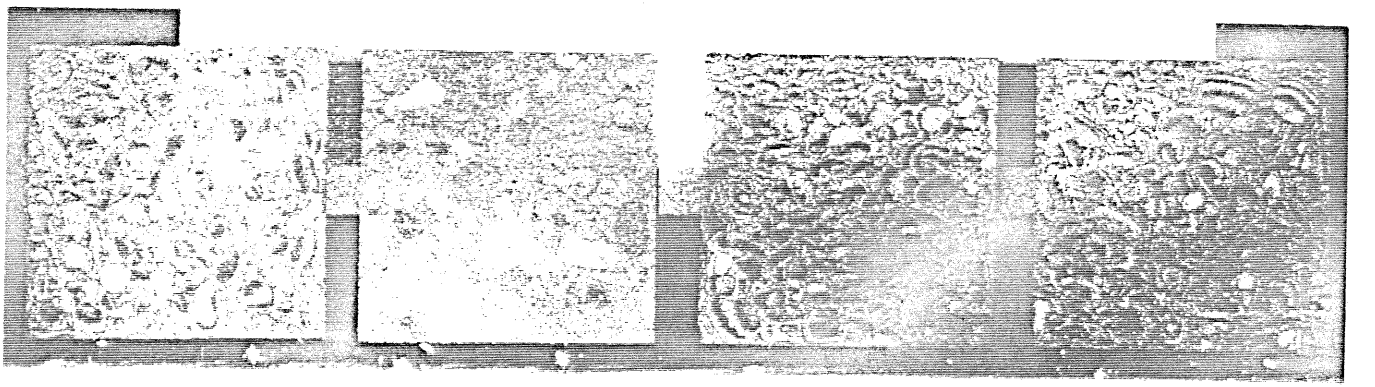

Fig: 3

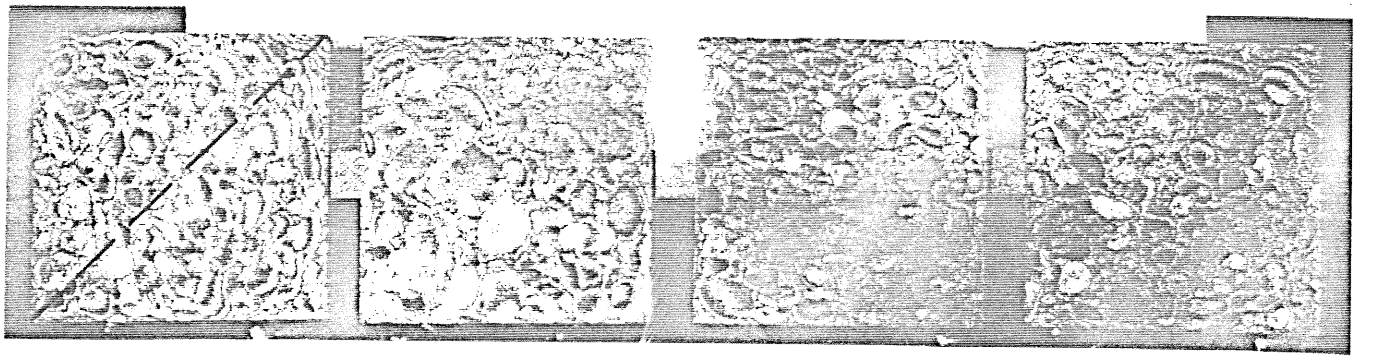

Fig: 4

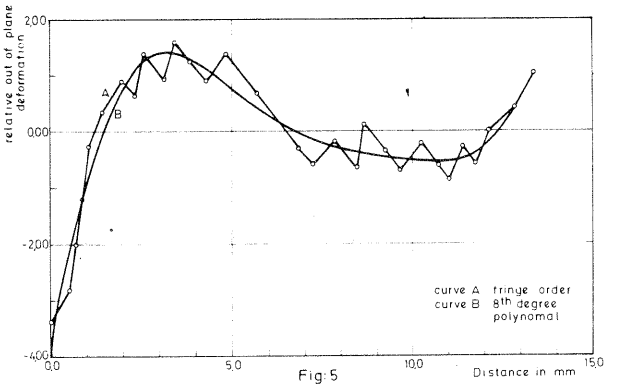

Fig: 5

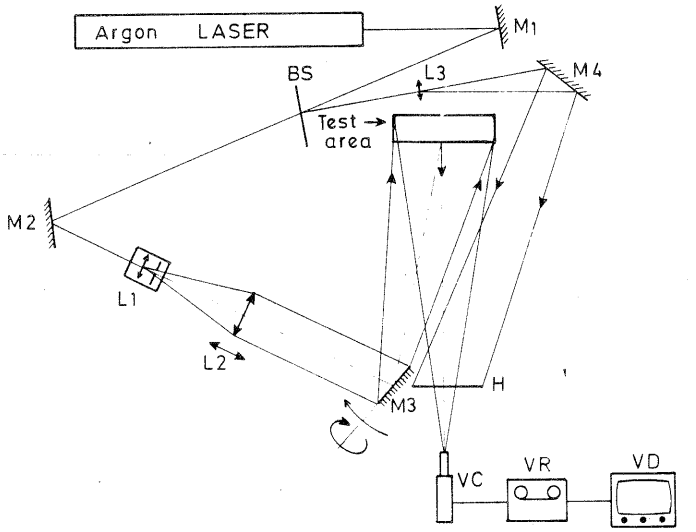

Fig: 6

Fig: 7a

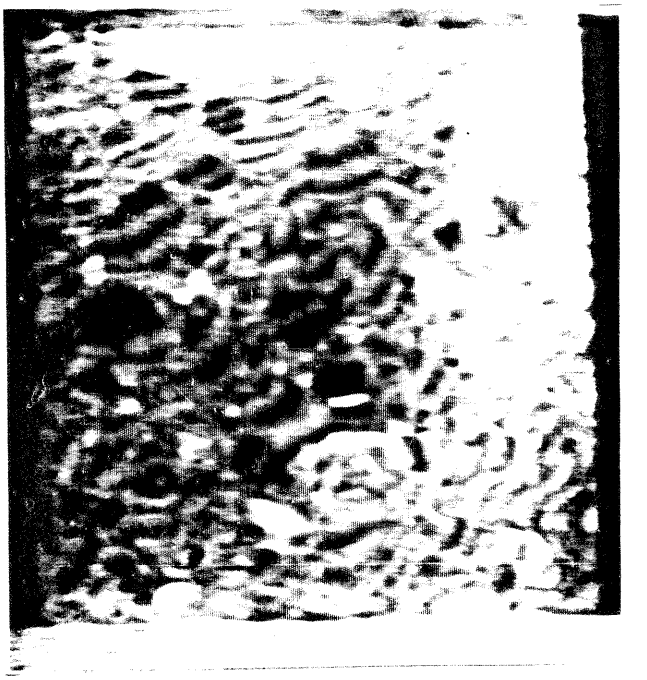

Fig: 7b

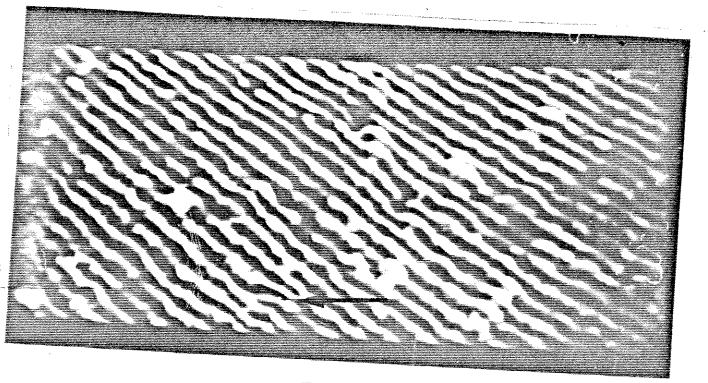

Fig: 8

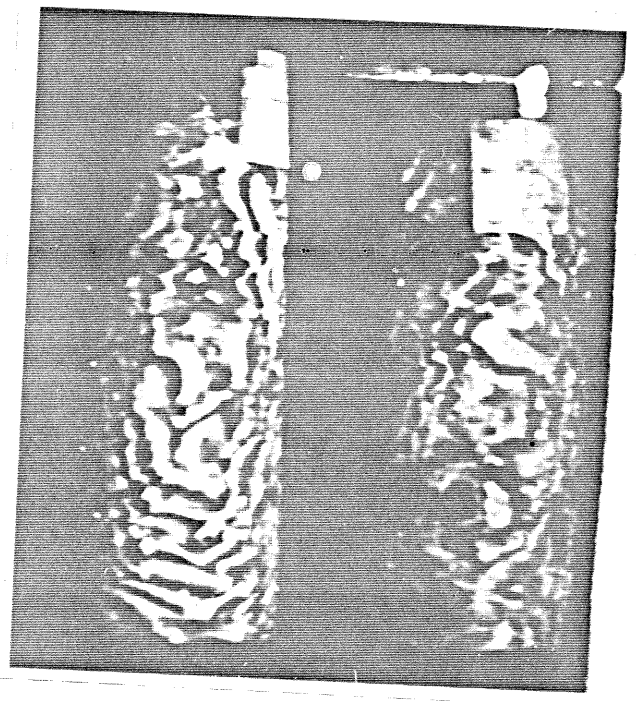

Fig: 9

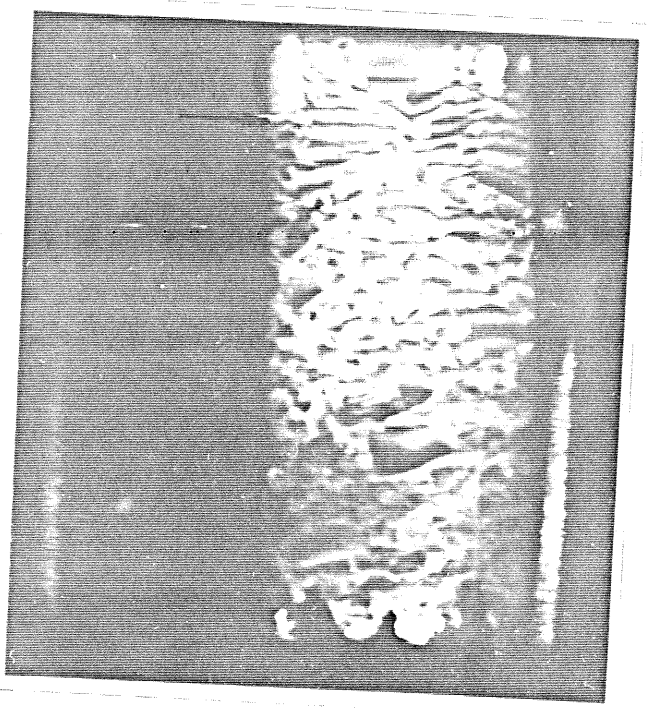

Fig: 10

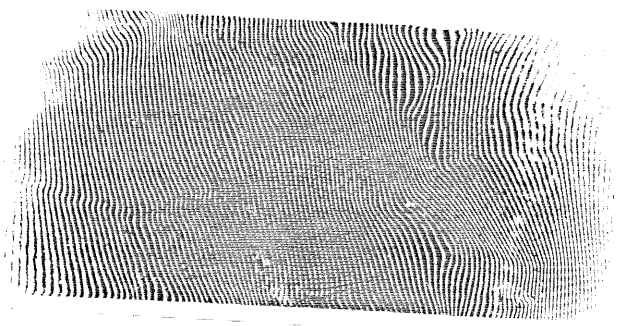

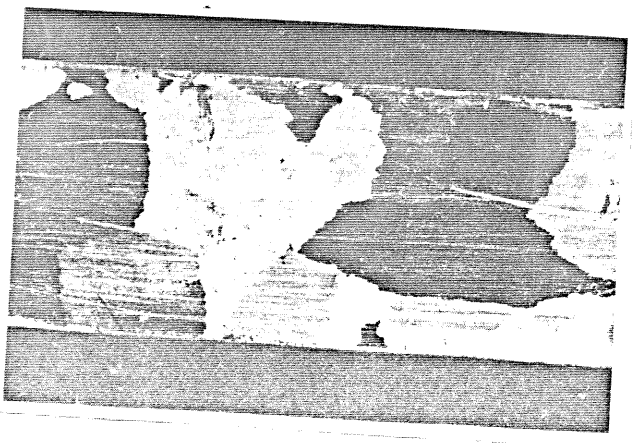

Fig: 11